Macrophage-derived granulin drives resistance to immune checkpoint inhibition in metastatic pancreatic cancer

Valeria Quaranta[1], **Carolyn Rainer**[1], **Sebastian R. Nielsen**[1], **Meirion L. Raymant**[1], **Muhammad S. Ahmed**[1], **Dannielle D. Engle**[2], **Arthur Taylor**[3], **Trish Murray**[3], **Fiona Campbell**[1], **Daniel H. Palmer**[1], **David A. Tuveson**[2,4], **Ainhoa Mielgo**[1], and **Michael C. Schmid**[1,*]

[1]Department of Molecular and Clinical Cancer Medicine, University of Liverpool, Ashton Street, Liverpool, L69 3GE, UK

[2]Cold Spring Harbor Laboratory, Cold Spring Harbor, NY 11724, USA

[3]Department of Cellular and Molecular Physiology, University of Liverpool, Ashton Street, Liverpool, L69 3GE, UK

[4]Lustgarten Pancreatic Cancer Research Laboratory, Cold Spring Harbor, NY 11724, USA

Abstract

The ability of disseminated cancer cells to evade the immune response is a critical step for efficient metastatic progression. Protection against an immune attack is often provided by the tumor microenvironment that suppresses and excludes cytotoxic CD8^{+} T cells. Pancreatic ductal adenocarcinoma (PDAC) is a highly aggressive metastatic disease with unmet needs, yet the immunoprotective role of the metastatic tumor microenvironment in pancreatic cancer is not completely understood. In this study we find that macrophage-derived granulin contributes to cytotoxic CD8^{+} T cell exclusion in metastatic livers. Granulin expression by macrophages was induced in response to colony-stimulating factor-1. Genetic depletion of granulin reduced the formation of a fibrotic stroma, thereby allowing T cell entry at the metastatic site. While metastatic PDAC tumors are largely resistant to anti-PD-1 therapy, blockade of PD-1 in granulin-depleted tumors restored the anti-tumor immune defense and dramatically decreased metastatic tumor burden. These findings suggest that targeting granulin may serve as a potential therapeutic strategy to restore CD8^{+} T cell infiltration in metastatic PDAC, thereby converting PDAC metastatic tumors, which are refractory to immune checkpoint inhibitors, into tumors that respond to immune checkpoint inhibition therapies.

Introduction

The ability of the immune system to identify and destroy cancer cells is a primary defense mechanism against cancer. CD8^{+} cytotoxic T cells, also known as cytotoxic T cells (CTLs), are key effectors of the immune response against cancer (1) and their presence in tumors is

Corresponding author: Michael C. Schmid, University of Liverpool, Ashton Street, Sherrington Building rm. 140, Liverpool L69 3GE, UK. mschmid@liverpool.ac.uk.

associated with a good clinical outcome in many tumor types, including ovarian, colon, breast, and pancreatic cancer (2–4). The importance of effector CD8^{+} T cell mediated anti-tumor immune response in oncogenesis is demonstrated by the clinical success of immunotherapies (1,5). Particularly, the use of immune checkpoint inhibitors has recently been shown to be beneficial for many types of cancers, with anti-programmed cell death protein 1 (PD-1) inhibitors being one of the leading candidates (6). However, immune checkpoint inhibitors only work if CD8^{+} T cells are infiltrated in to tumors. Pancreatic tumors are particularly poorly infiltrated by CD8^{+} T cells and thus, inhibition of immune checkpoint receptors alone did not show any benefit in pancreatic cancer patients (7,8). Pancreatic cancer is characterized by a rich and desmoplastic tumor stroma, also called tumor microenvironment (TME), identified by high numbers of activated fibroblasts, collagen deposition, and extensive myeloid cell infiltration, which all together critically impact the disease progression (9) and its response to therapy (10–12). The TME is also thought to be a major barrier to CD8^{+} T cell infiltration in pancreatic tumors (13,14) and it is necessary to overcome this immune/fibrotic-protective barrier for the successful use of immune checkpoint inhibitors (15,16).

Macrophages represent a major component of tumor infiltrating immune cells and depending on the activation signals, macrophages can acquire a spectrum of phenotypic states. In respect to cancer, macrophages can be polarized into M1-like inflammatory macrophages that activate a tumoricidal immune response (hereafter also referred to as M1-like), or into anti-inflammatory, immunosuppressive macrophages (hereafter also referred to as M2-like) that potently suppress other anti-tumor immune effector cells and thereby promote tumor progression (15,17,18). High density of macrophages, especially those exhibiting an immunosuppressive M2-like phenotype, correlates with poor clinical outcome in most human cancers (17). Accordingly, inhibition of myeloid cell recruitment into tumors have resulted in increased CD8^{+} T cell infiltration and decreased tumor burden in mouse models and early-phase clinical trials (15,18–23). Yet, the mechanisms by which macrophages regulate T cell infiltration is only beginning to emerge.

Pancreatic ductal adenocarcinoma (PDAC) is a very aggressive metastatic disease. Currently, surgical resection is the best treatment option for PDAC patients, but, unfortunately, by the time PDAC is diagnosed, the majority of patients (~ 80%) present with non-resectable metastatic cancer. Moreover, more than 60% of the patients whose tumors are removed, relapse with distant hepatic recurrence within the first 24 months after surgery (12,24). Thus, a better understanding of the mechanisms underlying the metastatic process in pancreatic cancer is critical to improve treatment and patient survival. We and others have recently identified that a desmoplastic TME also exists at the metastatic site in PDAC, which is mainly the liver, and that this fibro-inflammatory reaction is required for metastatic growth (25,26). However, whether and how the metastatic TME affects CD8^{+} T cell infiltration and function in the metastatic liver remains unexplored. Here, we found that macrophage-derived granulin is a key protein that supports CD8^{+} T cell exclusion and resistance to anti-PD-1 (αPD-1) treatment. In fact, we show that depletion of granulin converts PDAC metastatic tumors, which are refractory to anti-PD1 treatment, into tumors that respond to αPD-1. Our findings provide pre-clinical evidence that support the rational for targeting

granulin in combination with the immune checkpoint blocker PD-1 for the treatment of metastatic PDAC.

Material and Methods

Cells

Murine pancreatic cancer cells KPC FC1199, from here on referred as KPC, were generated in the Tuveson lab (Cold Spring Harbor Laboratory, New York, USA) isolated from PDA tumor of $Kras^{G12D/+}$; $p53^{R17H/+}$; Pdx1-Cre mice of a pure C57BL/6 background and authenticated as previously reported (27). The murine C57BL/6 Panc02 pancreatic ductal carcinoma cell line was obtained from the NCI DCTD Tumor Repository, NIH. $Panc02^{luc/zsGreen}$ or $KPC^{luc/zsGreen}$ cells were generated by using pHIV Luc-zsGreen (gift from B. Welm, University of Utah, USA, Addgene plasmid no.39196) lentiviral particle infection. Infected cells were selected for high zsGreen expression levels using flow cytometry cell sorter (ARIA, BD). Immortalized hepatic stellate cells were obtained by isolating hepatic stellate cells from $p21^{-/-}$ mice (C57BL/6), kindly provided by T. Sakai's laboratory, University of Liverpool, UK and were authenticated as previously described (28).

All cells were maintained at a minimal passage number (< p8) to allow initial expansion prior to use for *in vitro* and *in vivo* experiments. All cells were routinely tested negative for the presence of mycoplasma contamination. None of the cell lines used in this manuscript is listed in the ICLAC and NCBI Biosample database of misidentified cell lines.

Mice

6-8 weeks old female C57BL/6 mice were purchased from Charles River. $Grn^{-/-}$ mice (B6(Cg)-$Grn^{tm1.1Aidi}$/J) and tdTomatoRed mice (B6.129(Cg)-Gt(ROSA)26Sor$^{tm4(ACTB-tdTomato,-EGFP)Luo}$/J) both on the C57BL/6 genetic background were purchased from The Jackson Laboratory. $Kras^{G12D/+}$; $p53^{R172H/+}$; Pdx1-Cre mice were purchased from CRUK, Cambridge Research Institute, Cambridge.

All animal experiments were performed in accordance with current UK legislation under an approved project license PPL 40/3725 (M.C. Schmid). Mice were housed under specific pathogen-free conditions at the Biomedical Science Unit at the University of Liverpool. For tumor studies, female animals age 6-8 weeks were used. Animals were randomly assigned to experimental groups. The investigators were not blinded to allocation during experiments and outcome assessments.

In vivo animal studies

Liver experimental metastasis was performed by implanting 1×10^6 KPC $^{luc/zsGreen}$ or Panc02 $^{luc/zsGreen}$ in 25 μl PBS into the spleen of immunocompetent isogenic C57BL/6 mice using a Hamilton 29 G syringe as previously described (25,26). For selected experiments, macrophages were depleted using CSF-1 neutralizing antibody (BioXCell, clone 5A1,) or CSF-1R inhibitor (Selleckchem, BLZ945). Anti-CSF-1 antibody was administered via intraperitoneal (i.p.) injection every 5 days with the first injection containing 1 mg and subsequent injections containing 0.5 mg for a total of 3 injections in 14 days (early time

point treatment, d7) and 2 injections in 10 days (late time point treatment, d14) . Rat IgG1 (BioXCell, clone HRPN) was used as isotype control. CSF-1R inhibitor BLZ945 was administered daily at a concentration of 200 mg/kg in 20% Captisol (Ligand Pharmaceuticals) by oral gavage. 20% Captisol was used as vehicle control. For immune checkpoint blockade, PD-1 antagonist (BioXCell, clone RMP-1) or Rat IgG2 (BioXCell, clone 2A3) isotype control were administered every 3 days by i.p. injection at 250 µg/dose for a total of 4 injections in 14 days (early time point treatment, d7) and 3 injections in 10 days (late time point treatment, d14). In the experiments in which CSF-1 and PD-1 inhibitory antibodies have been used in combination, αPD-1 treatment was started 3 days after the first dose of CSF-1 inhibitor. For T-cell depletion study, anti-CD8 (αCD8, BioXCell, clone 2.43, 200 µg/dose) was injected by i.p. 2 days prior intrasplenic implantation of KPC$^{luc/zsGreen}$ cells into mice on the day of KPC$^{luc/zsGreen}$ implantation followed by injections every 4 days for the duration of the experiment. As isotype control, Rat IgG2 (BioXCell, clone LTF-2; 200ug/dose) was used. To validate the effect of hypoxia in metastatic liver mice, Digoxin (Sigma Aldrich) was used at concentration of 2 mg/kg by i.p. for a total of 2 injections in 3 days. To target fibrosis, Calcipotriol (Tocris Bioscience) was administered daily by i.p. injection at a concentration of 60 µg/kg for a total of 10 days. PD-1 antagonist (BioXCell, clone RMP-1, 250 µg/dose) treatment regimen was started after 3 Calcipotriol injections and continued for 10 days with an injection every 3 days. To assess the presence of hypoxic area in healthy and metastatic livers, the Hypoxyprobe™ RED 549 Kit (Hypoxyprobe, hpi) was used according to the manufacturer's instruction. Briefly, 1.5 mg/mouse of Hypoxtprobe™-1 (pimonidazole HCl) solution was administered via i.p.. Livers from injected mice were harvested after 60 min and stained with RED 549 dye-Mab1, a dye conjugated mouse IgG$_1$ monoclonal antibody. Treatment trials were initiated when transplanted tumors reached a mean volume of approximately 40 mm^3 and 180 mm^3 7 and 14 days after implantation, respectively. Time points for treatment analysis were preselected based on the expected window of efficacy (after 1-2 weeks of treatment).

Metastatic tumor burden quantification

Liver metastatic tumor burden was assessed, both *in vivo* and *ex-vivo,* by measuring bioluminescence signal (IVIS, Perkin Elmer) generated by KPC$^{luc/zsGreen}$ or Panc02 $^{luc/zsGreen}$ cells. Bioluminescence signal was detected by intraperitoneal injection (i.p.) of Beetle luciferin (Promega; 3 mg/mouse) and quantified as total flux (photons/sec). For some experiments, change in tumour volume in response to inhibitory Abs or drug treatment was assessed by 9.4 Tesla (T) horizontal bore Biospec MRI scanning (Bruker Biospin, Inc.). Mice livers were scanned *in vivo* before and after treatment using a T2-TurboRARE acquisition protocol. MRI images were acquired in coronal plane with 0.5 mm thickness and 0.1 mm spacing between each slice. A set of 23 slices was acquired to monitor the entire liver volume. Metastatic tumor volume was quantified by Image J software. Percentage change in metastatic tumor burden (before and after treatment) was obtained by calculating the sum of tumor area of all slices spanning the liver and multiplying it by 0.6 mm (inter-slice distance). The MRI acquisition used the following parameters: 2500 ms TR; 24 ms TE; 30x30 mm FOV; 240 x 240 image size. At indicated endpoints, liver metastatic lesions size and frequency were quantified based on haematoxylin and eosin staining of paraffin-embedded liver sections. Zeiss microscope and ZEN imaging software was used.

Preparation of conditioned media (CM)

Conditioned medium from Panc02, KPC cancer cells, bone marrow derived macrophages (BMM) and activated immortalized hepatic stellate cells (HSC) was generated according to previous reports (26). Briefly, the medium was removed from 70 % confluent cells and the cells were washed three times with PBS before addition of serum-free medium. Cells were incubated for 18-24h in serum-free medium and then collected and filtered through 0.45 μm filters before use.

Granulin gene expression analysis in bone marrow derived macrophages (BMMs)

Primary murine macrophages were generated by flushing the bone marrow from the femur and tibia of C57BL/6 mice followed by incubation for five days in DMEM containing 10 % FBS and 10ng ml^{-1} murine M-CSF (Peprotech). BMM were subsequently stimulated with DMEM containing 2% serum in the presence or absence of murine recombinant M-CSF (Peprotech) for 24 hour. Alternatively, BMMs were stimulated with KPC or Panc02 CM for 24 hours in the presence of absence of αCSF-1 inhibitory antibody (BioXCell; [2.5 μg/ml]). BMMs were finally lysed in RLT buffer + β-Mercaptoethanol and *Granulin* expression was assessed by qPCR.

ELISA

Assessment of granulin secretion—Primary murine bone marrow macrophages (BMMs) were generated as described above and subsequently stimulated with DMEM containing 2 % serum in the presence of murine recombinant M-CSF ([20 ng/ml]; Peprotech), IFNγ [20 ng/ml] and LPS [100 ng/ml (Peprotech and Sigma Aldrich, respectively), IL-10 ([20 ng/ml]; Peprotech), IL-13 ([20 ng/ml]), IL-4 ([20 ng/ml]; Peprotech) for 24 hours. Supernatant was collected to assess granulin protein level by ELISA (LifeSpan BioScience, LSBio). For assessing granulin secretion under hypoxic culture conditions, BMMs were maintained at 37 °C with 5% CO_2 and 1% O_2 (Don Whitley Scientific, Shipley, UK; Hypoxystation-H35). In all other cases, BMM were cultured under normoxic conditions (37 °C with 5 % CO_2 and ~18-21 % O_2). BMMs were cultured for 24 hours under normoxic and hypoxic conditions in the presence or absence of 10 ng/ml murine recombinant CSF-1 (Peprotech). For Dimethyloxaloylglycine (DMOG) treatment, cells were culture under normoxia condition in media supplemented with 0.5 mM DMOG (Enzo Laboratories, Farmingdale, NY, USA) for 24 hours. Supernatant was collected to assess granulin protein level by ELISA (LifeSpan BioScience, LSBio).

Assessment of M-CSF-1 secretion—Conditioned media from Panc02, KPC cancer cells and BMMs was obtained to measure the production of murine M-CSF by Quantikine ELISA kit (R&D System) according to the manufacturer's instruction.

Adoptive transfer experiments

For T cell adoptive transfer, experimental metastasis was induced by intrasplenic implantation of 1x10^6 KPC$^{luc/zsGreen}$ cells into tdTomatoRed+, WT, and Grn$^{-/-}$ mice. After 13 days, tumor bearing tdTomatoRed+ mice were euthanized and spleens were dissected to isolate CD8$^+$ T cells (Miltenyi, CD8a$^+$ T cell isolation Kit). Isolated CD8$^+$ T cells were

stimulated with Dynabeads Mouse T- Activator CD3/CD28 (Life Technology) following manufacturer's instruction, and incubated for 24 hours at 37°C. The next day, 1.5×10^6 tdTomoatoRed$^+$ CD8$^+$ T cells were injected into the tail vein of tumor bearing WT and Grn$^{-/-}$ mice. After 24 hours, mice were sacrificed and livers were collected and embedded in Optimal Cutting Temperature (OCT) medium. 5 μm liver sections were stained for DAPI (Life Technology, 1:500) and spatial localization of adoptive transferred dtTomatoRed$^+$ CD8+ T cells was assessed by fluorescence microscopy measuring dtTomato Red$^+$ signal.

For MAMs adoptive transfer, experimental metastasis was induced by intrasplenic implantation of 1×10^6 KPC$^{luc/zsGreen}$ cancer cells. Mice were treated with CSF-1 and PD-1 inhibitory Abs starting 7 or 14 days after cancer cells implantation. At day 24, metastatic livers from sacrificed mice were dissected to isolate F4/80$^+$ cells (Miltenyi, F4/80$^+$ isolation Kit). 1×10^6 F4/80$^+$ isolated cells were then injected into the tail vein of mice bearing experimental metastasis at day 7. After 5 days, injected mice were euthanized and liver were harvested and analyzed further.

Bone marrow transplantation

Bone marrow transplantation was performed by reconstituting the bone marrow of lethally irradiated (10 Gy) female, 6-week-old C57BL/6 mice by tail vein injection of 5×10^6 total bone marrow cells isolated from Grn$^{-/-}$ mice or WT mice. After 4 weeks, engraftment of Grn$^{-/-}$ bone marrow was assessed by genomic DNA PCR according to The Jackson Laboratory protocol on peripheral blood cells from fully recovered bone-marrow-transplanted mice. After confirmation of successful bone marrow reconstitution, mice were enrolled in tumour studies.

Flow cytometry and cell sorting

Single cell suspensions from murine livers were prepared by mechanical and enzymatic disruption in Hanks Balanced Salt Solution (HBSS) with 1 mg/mL Collagenase P (Roche) as previously described (26). Briefly, cell suspensions were centrifuged for 5 minutes at 1200 rpm, resuspended in HBSS and filtered through a 500 μm polypropylene mesh (Spectrum Laboratories). Cell suspensions were resuspended in 1ml 0.05 % trypsin and incubated at 37° C for 5 minutes. Cells were filtered through a 70 μm cell strainer and resuspended in PBS + 0.5% BSA. Cells were blocked for 10 minutes on ice with FC block (BD Pharmingen, Clone 2.4 G2,) and then stained with Sytox-blue viability marker (Life Technologies) and conjugated with antibodies against CD45 (Clone 30F-11), F4/80 (Clone BM8), CD8 (Clone 53-6.7), CD206 (Clone C068C2), PD-1(Clone 29F.1A12), CD69 (Clone H1.2F3), CD3 (Clone 145-2C11), CD11b (Clone M1/70), Ly6C (Clone HK 1.4), Ly6G (Clone 1A8), IFNγ (Clone XMG1.2), Ki67 (Clone 16A8); Ly6G (Clone 1A8) all purchased from Biolegend; Granzyme B (eBioscience, clone NGZB). For intracellular staining, cells were first fixed (eBioscience, IC fixation buffer) and permeabilized (eBioscience, 1x permeabilization buffer).

To assess IFNγ expression levels in metastasis derived CD8$^+$ T cells, magnetically isolated CD8a$^+$ T cells from metastatic livers were stimulated with 50 ng/ml phorbol 12-myristate 13- acetate (PMA) (Sigma Aldrich) and 1 μg/ml of Ionomycin (Sigma Aldrich) for 5 hours

at 37° C in the presence of Brefeldin A (eBioscience, 1:100) and subsequently stained for IFNγ.

Flow cytometry was performed on a FACS Canto II (BD Bioscience) and FACS cell sorting was carried out using FACS Aria (BD Bioscience). Cells were sorted directly in RLT buffer + β-Mercaptoethanol accordingly with the manufacturer's instruction for RNA isolation (Qiagen).

Magnetic beads isolation of cells

Samples for magnetic bead isolation were prepared from livers as described above for preparation of flow cytometry samples. Samples were stained and CD8a$^+$ or F4/80$^+$ cells were isolated according to the manufacturer's instruction (Miltenyi).

In vitro T-cell activation assay

Primary splenocytes were obtained from spleens of naïve C57BL/6 mice. Dissected spleens were dissociated in MAC buffer and passed through a 70 μm cell strainer to obtain a single cell suspension. Cells were centrifuged (400 x g) and red blood cells were lysed using 1x Red blood lysis buffer (Biolegend). Obtained splenocytes were cultured in RPMI supplemented with 10% FBS. For T cell activation assays, splenocytes were stimulated using Dynabeads Mouse T- Activator CD3/CD28 (Life Technology). Activated splenocytes (S) were then co-cultured with bone marrow derived macrophages (BMMs) from WT and Grn$^{-/-}$ mice or with macrophages (M) magnetically isolated cells from day 6 and day 14 metastasis bearing livers (4:1 ratio, S: M). Cells were plated in 96 well plates and incubated at 37°C for 24h. Subsequently, Brefeldin A (eBioscience, 1:100) was added to the cells for 5h. Cells were then harvested and stained with CD8 (Biolegend, clone 53-6.7) and IFNγ (Biolegend, Clone XMG1.2) antibodies and analyzed by flow cytometry. For some experiments, recombinant mouse Progranulin protein (recGrn) (R&D systems; [1 μg/ml]) and mouse Periostin neutralizing antibody (R&D systems; [1 μg/ml]) were used.

In vitro T- cell proliferation Assay

For T cell proliferation assay, splenocytes derived from naïve C57BL/6 mice were labelled with 5 μM Carboxyfluorescein Diacetate Succinimidyl Ester (CFSE) (Biolegend) and incubated for 10 minutes at 37°C in the dark. Cells were then resuspended in RPMI 1640 supplemented with 10% FBS and stimulated with Dynabeads Mouse T-Activator CD3/ CD28. Activated splenocytes (S) were then co-cultured with bone marrow derived macrophages (BMMs) from WT and Grn$^{-/-}$ mice or with macrophages (M) magnetically isolated cells from day 6 and day 14 metastasis bearing livers (4:1 ratio, S: M). Cells were plated in 96 well plates and incubated at 37°C for 72 hours. Subsequently, cells were harvested and stained with CD8 antibody (Biolegend, clone 53-6.7). Proliferating CD8+ T cells were tracked by flow cytometry. For some experiments, recombinant mouse Progranulin protein (R&D systems; [1 μg/ml]) and mouse Periostin neutralizing antibody (R&D systems, [1 μg/ml]) were used.

RT-qPCR

Total RNA purification was performed with the RNeasy kit (Qiagen) and cDNA was generated using QuantiTect Reverse Transcription kit (Qiagen) according to the manufacturer's instructions. 500 ng of total RNA was used to generate cDNA. Quantitative polymerase chain reaction (qPCR) was performed using 5x HOT FIREPol EvaGreen qPCR Mix Plus (ROX) (Solis Biodyne) on an MX3005P instrument (Stratagene). Three-step amplification was performed (95° C for 15 seconds, 60° C for 20 seconds, 72° C for 30 seconds) for 45 cycles. Relative expression levels were normalized to *Gapdh* expression according to the formula $2^{\wedge}-$ (Ct *gene of interest* – Ct *Gapdh*). Fold increase in expression levels were calculated by comparative Ct method $2^{\wedge}-$ (ddCt).

The following QuantiTect Primers Assays were used to assess mRNA levels: *Gapdh* (Mm_Gapdh_3_SG; QT01658692), *Cxcl10* (Mm_Cxcl10_1_SG; QT00093436), *Cd86* (Mm_Cd86_1_SG; QT01055250), *Ifng* (Mm_Ifng_1_SG; QT01038821), *Il12* (Mm_Il12b_1_SG; QT00153643), *H2-Aa* (Mm_H2-Aa_1_SG; QT01061858), *Retnla* (Mm_Retnla_1_SG; QT00254359), *Tgfb* (Mm_Tgfb1_1_SG; QT00145250), *Il10* (Mm_Il10_1_SG; QT00106169), *Arginase* (Mm_Arg1_1_SG; QT00134288), *Gzmb* (Mm_Gzmb_1_SG; QT00114590), *Tnf* (Mm_Tnf_1_SG; QT00104006), *Prf1* (Mm_Prf1_1_SG; QT00282002), *Mrc1* (Mm_Mrc1_SG; QT00103012), *Granulin* (Mm_Grn_1_SG; QT01061634). All primers were purchased from Qiagen.

Immunofluorescence

Murine liver tissues were fixed using a sucrose gradient method to preserve the zsGreen fluorescence. Briefly, livers were fixed in 4% Formaldehyde + 10% sucrose in PBS for 4 hours and then transferred to 20% sucrose in PBS for 8-10 hours. Tissues were transferred into 30% sucrose for an additional 8-10 hours, embedded in OCT medium and stored at -80°C.

For immunofluorescence staining 5 μm liver sections were permeabilized by 0.1% TritonX-100 (Sigma Aldrich) for 10 minutes. Unspecific bindings were prevented by using PBS +8% Normal goat serum for 1 hour at RT. Tissue sections were incubated overnight at 4 °C with the following antibodies: αSMA (Abcam, ab5694, 1:100); Relm-α (Abcam, 39626, 1:100); Cleaved- Caspase 3 (Cell Signalling, 9661, 1:100); CSF1R (Santa Cruz Biotechnology, clone c-20, 1:100). The next day, tissue sections were washed in PBS and stained with the secondary antibody goat anti-rabbit conjugated to AlexaFluo594 (Abcam, 1:500) and DAPI (Life Technologies, 1:500) for 1 hour at RT. Zs Green/Luciferase transfected cells were detected by their intrinsic signal. Sections were finally mounted using Dako Fluorescent Mounting Medium.

Immunofluorescence staining was also performed in some cases on tissue sections obtained from livers directly embedded in OCT. In this case tissue sections were fixed in ice-cold acetone for two minutes and permeabilized with 0.1% TritonX-100. Sections were washed and incubated overnight at 4°C with the primary antibodies: CD8 (Biolegend, clone 53-6.7, 1:100), F480 (Biolegend, clone BM8, 1:100). The next day, tissue sections were washed in PBS and stained with the secondary antibody goat anti-rabbit conjugated to AlexaFluo594

(Abcam, 1:500); goat anti-rat conjugated to AlexaFluo488 (Abcam, 1:500) and DAPI (Life Technologies, 1:500) for 1 hour at RT. All tissue sections were imaged using an Axio Observer Light Microscope with the Apotome.2 (Zeiss) and quantified using the Zen Software (Zeiss). Quantification of intrametastatic (IM) and peripheral (P) CD8$^+$ T cells was performed using Nis Elements, Advanced Research software (Nikon). Peripheral area of metastatic lesions was defined as the outer 40 % of the total lesion area.

Immunohistochemistry analysis

Deparaffinization and antigen retrieval was performed using an automated DAKO PT-link. Paraffin-embedded human and mouse liver metastatic sections were immunostained using the DAKO envision+system-HRP. Tissue sections were incubated overnight at 4°C with primary antibodies: αSMA (Abcam, ab5694, 1:200); CD8 (Dako, Clone 144b, 1:100); Cytokeratin 19 (Abcam, ab53119, 1:100); Granzyme B (Dako, 1:50); PD-1 (CD279) (Abcam, ab52587, 1:100); CD3 (Abcam, ab16669, clone SP7, 1:100); Granulin (R&D Systems, MAB25571, 1:50); iNOS (Abcam, ab15323, 1:100); MHC II (Abcam, ab25333, 1:100); COX-2 (Cambridge bioscience, aa570-598, 1:100); Ym-1 (StemCell Technology, 60130, 1:200); CD206 (Abcam, ab8918, 1:100); Ly6G (Biolegend, Clone A18, 1:100); B220 (Biolegend, 103202, 1:50). Secondary-HRP conjugated antibodies were incubated for 30 minutes at RT. Staining was developed using diaminobenzidine and counterstained with hematoxylin. For CD8 staining VECTASTAIN® Elite® ABC-HRP Kit (Peroxidase, Rat IgG) (Vector laboratories) was used.

Picrosirius red staining

Paraffin embedded murine liver samples were de-waxed and hydrated using a graded ethanol series. Tissue sections were then treated with 0.2% phosphomolybdic acid and subsequently stained with 0.1 % Sirius red F3B (Direct red 80)(Sigma Aldrich) in saturated picric acid solution for 90 minutes at RT. Tissues were then rinsed twice in acidified water (0.5% glacial acetic acid) (Sigma Aldrich) before and after the staining with 0.033 % fast green FCF (Sigma Aldrich). Finally, tissues were dehydrated in three changes of 100 % ethanol, cleared in xylene and mounted. Picrosirius red staining was quantified using Image J software.

Human tissue samples

Paraffin embedded human tissue sections from control healthy subjects, primary PDAC tumors and PDAC liver metastasis were obtained from the Liverpool Tissue Bank, University of Liverpool, UK. All patients were treatment naïve (no prior chemotherapy). Patient samples were collected after obtaining written informed consent from patients under the frame of the Declaration of Helsinki. All samples were pathologically confirmed. All studies involving human tissues were approved by the University of Liverpool and by National Research Ethics (Research Integrity and Governance Ethics committee North West Cheshire Reference: REC15/NW/0477).

Statistical analysis

Statistical analysis of experiments with two groups was performed using a two-tailed unpaired Student's t-test with 95% confidence interval. Statistical analysis of experiments with more than two groups was performed using nonparametric analysis of variance (ANOVA) test with comparisons between groups using Bonferroni's multiple comparison test. All statistical analysis were performed using GraphPad Prism software, $p < 0.05$ was considered significant. Statistical significance is indicated in the figures as follows: ***, $p < 0.001$; **, $p < 0.01$; *, $p < 0.05$; n.s., not significant. Histograms are shown as mean ± SEM. The following numbers (n) of fields of views (FoV) were analyzed for each tissue section staining: Fig. 1A (n=3), Fig. 1C (n=5), Figs. 2 D-F (n=5), Fig. 3B (n=4), Fig. 4C (n=4), Figs. 4D-G(n=5), Figs. 5E,F (n=5), Figs. 6A,E (n=5), Figs. 7C,D (n=6), Supplementary Figs. S1A,B, (n=3), Supplementary Figs. S2B,D,E (n=5), Supplementary Fig. S3I (n=4), Supplementary Figs. S4F,G,H,I,J,L,M (n=5), Supplementary Figs. S5D-K (n=6), Supplementary Fig. S5P (n=4), Supplementary Figs. S6B-D (n=6), Supplementary Fig. S6E (n=4), Supplementary Figs. S6H-J (n=6), Supplementary Figs. S7 C,D (n=6), Supplementary Fig. S8C (n=3).

Results

CD8+ T cell function and infiltration are lost during metastatic progression

To investigate whether anti-tumor immunity might affect PDAC metastasis, we first analyzed by immunohistochemistry (IHC) technique liver biopsies from advanced metastatic PDAC patients, and healthy livers. In metastatic PDAC liver samples, large metastatic lesions with high numbers of cytokeratin positive (CK+) tumor cells (CK+ rich) showed few infiltrating CD8+ T cells. In contrast, smaller metastatic tumor deposits (CK+ poor) were rich in CD8+ T cells (Figs. 1A,B; Supplementary Fig. S1A). Similarly, small spontaneous metastatic lesions generated in Kras^G12D;Trp53^R172H;Pdx1-Cre (KPC) mice (27) showed higher CD8+ T cell infiltration compared to larger established lesions (Supplementary Fig. S1B).

To further evaluate the changes in CD8+ T cell infiltration during PDAC metastasis, we next induced liver metastasis by intrasplenic implantation of KPC-derived pancreatic cancer cells expressing the dual reporter gene zsGreen and firefly luciferase (KPC^zsGreen/luc) (25,26,29). In agreement with the data obtained in PDAC patients and the autochthonous KPC model, small metastatic lesions, mainly found at the early stage of metastatic progression (6 days post intrasplenic implantation, d6) and characterized by low numbers of KPC cancer cells, showed high infiltration of CD8+ T cells in comparison to tumor free livers. In contrast, large metastatic lesions with abundant cancer cell numbers, mainly found at a later stage of metastasis progression (14 days post intrasplenic injection, d14), showed a significant loss of CD8+ T cells (Figs. 1C-E). To assess whether the identified CD8+ T cells were active, we next stained for the T cell activation marker CD69 and the inhibitory immune checkpoint receptor PD-1. CD8+ T cells from small tumors (d6) were active (CD69+ and PD-1-), while CD8+ T cells isolated from large metastatic tumors (d14) were inactive (CD69- and PD-1+) (Figs. 1F,G; Supplementary Fig. S1C). Gene expression analysis of the cytolytic factors *Tnfa* and *Gzmb* in metastasis infiltrating CD8+ T cells positive for PD-1 confirmed that the few

infiltrating CD8^{+} T cells in large metastatic lesion (day 14) were also exhausted (Fig. 1H). Collectively, these results indicate that CD8^{+} T cells are able to infiltrate small metastatic tumors but that during metastatic progression CD8^{+} T cell infiltration and cytotoxic function are lost.

Immunosuppressive M2-like metastasis associated macrophages (MAMs) accumulate during PDAC metastasis

Tumor and metastasis associated macrophages can restrict CD8^{+} T cell effector functions depending on their activation state (16,30). Since large numbers of metastasis associated macrophages (MAMs) can be found at the hepatic metastatic site in PDAC (26), we next analyzed gene expression of M1- and M2-like activation markers in isolated MAMs (Supplementary Fig 2A). While we did not observe a significant difference in MAM numbers (Fig. 2A), MAMs isolated from small metastatic tumors (d6) revealed higher expression of immune stimulatory genes (*C-X-C motif chemokine 10*, *Cxcl10*; *interleukin 12*, *Il2*; *interferon gamma*, *Ifng*) and genes associated with antigen presentation (*H2Aa; Cd86*), resembling a pro-inflammatory M1-like phenotype (Fig. 2B). In contrast, macrophages isolated from large metastatic tumors (d14) significantly upregulated the expression of immunosuppressive (transforming growth factor beta, *Tgfb*, *Arginase*, *Il10*) and anti-inflammatory M2-like markers (*mannose receptor C-type 1, Mrc1, resistin-like-α, Retnla*) (Fig. 2C). Analysis of small metastatic tumor tissue sections confirmed a higher number of myeloid-like cells expressing prototypical pro-inflammatory markers, including inducible nitric-oxide synthase (iNOS), major histocompatibility complex class II (MHC-II) and cyclooxygenase-2 (COX-2) (Fig. 2D). On the contrary, larger established metastatic tumors contained a higher number of myeloid-like cells expressing M2-like alternative activation markers, such as macrophage mannose receptor 1 (CD206) and Chitinase-like protein 3 (Ym-1) (Fig. 2E), and M2-like (RELMα[+]) MAMs accumulated in close proximity to disseminated cancer cells (zsGreen) (Fig. 2F).

Since M2-like macrophages can execute potent inhibitory effects on cytotoxic CD8^{+} T cell functions (30), we next explored the apoptotic rate of disseminated tumor cells. We observed a higher apoptotic rate (cleaved caspase 3^{+}) of cancer cells in small metastatic lesions (d6) compared to large metastatic lesions (d14) (Supplementary Fig. S2B). Moreover, MAMs isolated from established metastatic lesions significantly suppressed CD8^{+} T cell proliferation (Fig. 2G) and activation *ex vivo* (Fig. 2H), compared to MAMs isolated from small metastatic lesions.

Together, these data suggest that metastatic progression in PDAC is accompanied by the reprogramming of MAMs towards an M2-like immunosuppressive phenotype that can inhibit cytotoxic CD8^{+} T cell functions.

Pharmacological blockade of the CSF-1/CSF-1R axis reprograms MAMs towards an immune-stimulatory phenotype and restores CD8^{+} T cell mediated anti-tumor immunity in metastatic PDAC

Based on our findings, we reasoned that blocking the rewiring of M1-like MAMs into immunosuppressive M2-like MAMs during metastatic progression could sustain tumoricidal

CD8^{+} T cell functions and subsequently inhibit PDAC metastasis. Colony stimulating factor 1 (CSF-1) and its cognate receptor CSF-1R are among the most advanced targets to inhibit tumor promoting macrophage functions in cancer (19,31). CSF-1 is abundantly expressed by metastatic pancreatic cancer cells (Supplementary Fig. S2C) and CSF-1R is expressed by MAMs in experimental and spontaneous PDAC metastasis models (Supplementary Figs. S2D,E). To assess whether the inhibition of CSF-1 affects MAM functions, T cell infiltration/activation, and metastatic PDAC progression, we induced hepatic metastasis by intrasplencially implanting KPC cells. Starting at d7, we administered neutralizing anti-CSF-1 monoclonal antibody (αCSF-1) for 2 weeks (Fig. 3A). αCSF-1 treatment reduced metastatic tumor burden (Fig. 3B). In respect to MAMs, αCSF-1 reduced not only overall MAM numbers (Fig. 3C), but specifically reduced the number of M2-like F4/80^{+}CD206^{+} MAMs (Fig. 3D). Gene expression analysis of MAMs further confirmed that inhibition of CSF-1 induces a reprogramming of MAMs towards an inflammatory M1-like phenotype (Fig. 3E). Consistent with a rewired pro-inflammatory metastatic microenvironment, CD8^{+} T cell numbers and function were increased in αCSF-1 treated mice (Figs. 3F-I). It is noteworthy that αCSF-1 treatment also enhanced the proliferation rate (Ki67^{+}) within PD-1^{+}CD8^{+} T cells, suggesting a partial reinvigoration of exhausted PD-1^{+} CD8^{+} T cells within the metastatic niche (Fig. 3J). Tumor bearing mice treated with a small molecule inhibitor of CSF-1R (BLZ945) (32) showed a similar reduction in the metastatic tumor burden (Supplementary Figs. S3A-E) accompanied by an increase of pro-inflammatory M1-like MAMs (Supplementary Figs. S3F,G) and CD8^{+} T cells in metastatic livers (Supplementary Fig. S3H), and an increase in apoptosis of metastatic cancer cells (Supplementary Fig. S3I) *in vivo*.

Pharmacological depletion of CD8^{+} T cells abolished the anti-metastatic effect of αCSF-1 (Fig. 3K; Supplementary Figs. S3J,K) demonstrating that the ability of MAMs to support PDAC metastasis is in part due to their capacity to suppress cytotoxic CD8^{+} T cells.

Taken together, our findings show that MAM targeted therapies can restore a pro-inflammatory environment in metastatic PDAC in which cytotoxic CD8^{+} T cells can infiltrate and kill metastatic cancer cells.

CSF-1 inhibition reduces desmoplasia and sensitizes metastatic PDAC to αPD-1 treatment

Since αCSF-1 restores T cell infiltration in metastatic tumors (Fig. 3) we next evaluated whether αPD-1 treatment could further improve the anti-tumorigenic effect of αCSF-1. To test this, we treated tumors early (d7), or later (d14), after T cell infiltration is lost (Fig. 1; Fig. 4A). In response to early intervention (d7), metastatic tumour progression was significantly inhibited by both agents delivered as monotherapies (αPD-1=49 ±3%; αCSF-1=50+/-3%), but the anti-tumorigenic effect of αCSF-1 treatment was further potentiated when administrated in combination with αPD-1 (αCSF-1/αPD-1=80 ±3%) (Fig. 4B). In contrast, in response to a later intervention on larger metastatic lesions (d14), neither αPD-1 nor αCSF-1 alone was able to reduce metastatic tumor burden (KPC: αPD-1=3 ±3%; αCSF-1=22 ±2%; Panc02: αPD-1=5 ±3%; αCSF-1=21 ±4%) (Fig. 4B). In large metastatic lesions, only combinatorial treatment of αCSF-1/αPD-1 was able to reduce metastatic tumor burden by 61 ±4% (KPC) and 55 ±3% (Panc02), respectively (Fig. 4B).

Early intervention showed a better response (improved by an additional 20 ±8%) to combinatorial αCSF-1/αPD-1 therapy compared to later intervention. To address whether impaired drug delivery and/or the difference in treatment regimen might have caused the inferior response to therapy at the later intervention, we next directly compared the anti-tumoral activity of MAMs isolated from tumors exposed to αCSF-1 and αPD-1 early (starting d7) versus late (starting d14) intervention. The adoptive transfer of isolated MAMs reduced metastatic tumor progression (Supplementary Figs. S4A,B), increased the presence of M1-like MAMs and CD8$^+$ T cells (Supplementary Figs. S4C-E) in comparison to control mice which did not receive an adoptive transfer of MAMs. However, minimal differences were found between mice receiving MAMs from the early treatment versus late treatment, suggesting that the inferior effect of anti- αCSF-1/αPD-1 therapy at late intervention (compared to early intervention) was due to a more advanced stage of metastatic progression and to the poor infiltration of CD8$^+$ T cells observed in large lesions, and not due to an impairment in drug delivery or differences in treatment regimens.

Previous studies suggest that myofibroblasts and collagen deposition can impair T cell infiltration in primary tumors (14,33). Thus, we hypothesize that targeting MAMs by αCSF-1 treatment may decrease myofibroblast accumulation and collagen deposition, thereby supporting T cell infiltration and subsequently increase αPD-1 efficacy. To address this question we first assessed the spatial localization of CD8$^+$ T cells in advanced PDAC metastatic tumors from patients and mice. Advanced metastatic human tumors had low numbers of intra-metastatic CD8$^+$ T cells and the majority of CD8$^+$ T cells presented in these tumors accumulated at the periphery of metastatic lesions, where typically high numbers of myofibroblasts (αSMA$^+$) are found (Fig. 4C). Similar, large murine metastatic lesions (d14), showed an increase in αSMA$^+$ myofibroblasts, collagen deposition, that correlates with a decrease in CD8$^+$ T cell infiltration (Fig. 4D).

In line with our hypothesis, inhibition of CSF-1 altered the desmoplastic reaction at the metastatic site. In fact, KPC and Panc02 tumors treated with αCSF-1 alone or in combination with αPD-1 markedly reduced collagen deposition (Fig. 4E; Supplementary Figs. S4F-H), αSMA$^+$ myofibroblast numbers (Fig. 4F; Supplementary Figs. S4I,J), and increased CD8$^+$ T cell infiltration (Fig. 4G; Supplementary Figs. S5K-M) independently of the time of treatment intervention.

Taken together, these data suggest that reducing the fibrotic reaction by targeting macrophages increases CD8$^+$ T cell infiltration and response to αPD-1 therapy.

CSF-1 inhibition reduces granulin expression in macrophages *in vitro* and *in vivo*

We previously identified macrophage-derived granulin as a key effector protein for αSMA$^+$ myofibroblast accumulation during PDAC metastasis (26). Granulin is a secreted glycoprotein that stimulates fibroblast activation and migration (34,35). Thus, we next asked whether inhibition of CSF-1 could impair the expression of granulin in macrophages. We found that recombinant CSF-1 is a strong inducer of granulin expression in primary bone marrow derived macrophages (BMMs) (Fig. 5A) and that elevated granulin secretion correlates with alternatively (M2-like) activated macrophages (Supplementary Fig. S5A). Pancreatic cancer cells, which abundantly secrete CSF-1 (Fig. 5B), induced the expression

of granulin in macrophages in a CSF-1 dependent manner (Fig. 5C). Accordingly, macrophages isolated from αCSF-1 treated metastatic tumors have reduced granulin expression (Fig. 5D,E).

Hypoxia is a hallmark of cancer and hypoxia supports tumor promoting functions of macrophage (36,37). Thus, we next studied whether hypoxia affects granulin expression in macrophages during PDAC metastasis. Hypoxia progressively increased during PDAC metastasis (Fig. 5F). *In vitro* treatment with the chemical hypoxia mimetic dimethyloxaloglycine (DMOG) (38) or hypoxic culture conditions (1% O_2) increased granulin secretion by macrophages (Figs. 5G,H). Importantly, hypoxic culture conditions markedly amplified the granulin-inducing effect of CSF-1 (Fig. 5H). In an attempt to test the role of tumor hypoxia in increasing granulin expression *in vivo*, we treated tumor bearing mice with digoxin, a translational inhibitor of hypoxia-inducible factors 1 α (HIF-1α) (39). Administration of digoxin reduced metastatic tumor burden, prevented granulin expression, inhibited αSMA$^+$ myofibroblast accumulation, increased CD8$^+$ T cell numbers, and increased the presence of M1-like MAMs, while total MAM numbers remained unchanged (Supplementary Figs. S5B-K).

Taken together, these results demonstrate that CSF-1 induces granulin expression in macrophages, which can be further amplified under hypoxic conditions.

Genetic depletion of granulin restores CD8$^+$ T cell infiltration in metastatic tumors, but T cell dysfunctionality remains

Since inhibition of CSF-1 reduces granulin expression, we evaluated the effect of granulin depletion in regulating T cell infiltration. Therefore we intrasplenically injected KPC-derived cells into chimeric mice deficient of granulin (Grn$^{-/-}$) in the bone marrow (BM) compartment (WT+ Grn$^{-/-}$ BM mice). Intra-metastatic CD8$^+$ T cell accumulation was improved in granulin deficient mice (Figs. 6A,B) which are defective in myofibroblast activation (Figs. 6A,C). Moreover, by comparing metastatic lesions of equal sizes in WT and Grn$^{-/-}$ mice, we found an increase of adoptive transferred tdTomatoRed (tdTR) CD8$^+$ T cells in the intra-metastatic area of granulin deficient tumours compared to WT (Figs. 6D,E). Overall hematopoietic (CD45$^+$), T (CD3$^+$), neutrophil (Ly6G$^+$), macrophage (F4/80$^+$) and B (B220$^+$) cell numbers remained unchanged in granulin deficient metastatic tumours (Supplementary Figs. S5L-P). Although in granulin deficient mice we did not observe a difference in CD8$^+$ T cell numbers (Fig. 6F) nor in their activation state (Fig. 6G), we queried whether granulin might affect T cell functions directly or indirectly through the activation of hepatic stellate cells. Recombinant granulin did not have a direct effect on T cell functions *in vitro*, while macrophages lacking granulin retained their CD8$^+$ T cell suppressive capacity (Fig. 6H, I). In contrast, conditioned media collected from activated hepatic stellate cells reduced CD8$^+$ T cell activation (Fig. 6J) and proliferation (Fig. 6K).

Taken together, our results suggest that depletion of granulin improves CD8$^+$ T cell infiltration into metastatic tumors, but it does not directly affects their function.

Depletion of granulin restores the response of metastatic PDAC to αPD-1 therapy

To test whether the observed increase in CD8$^+$ T cell entry into granulin deficient metastatic tumors might improve their response to αPD-1 therapy, we treated tumor bearing WT and Grn$^{-/-}$ mice with either αPD-1 or IgG control antibody (Fig. 7A). Metastatic tumor burden was quantified by *in vivo* bioluminescence imaging (BLI) techniques at day 14 prior treatment and at endpoint (day 24). While single agent αPD-1 therapy did not show any efficacy in WT tumors, αPD-1 treatment in Grn$^{-/-}$ mice caused a dramatic decrease in metastatic progression, with even partial regression (Fig. 7B,C, Supplementary Fig. S6A). As expected, no changes in myofibroblast accumulation and CD8$^+$ T cell infiltration were detected in WT tumors in the presence or absence of αPD-1. In contrast, in Grn$^{-/-}$ tumors which are deficient in myofibroblast accumulation, CD8$^+$ T cell numbers significantly increased upon αPD-1 treatment (Figs. 7D-F). Moreover, αPD-1 treatment did not alter GzmB nor IFNγ expression levels in CD8$^+$ T cells isolated from WT tumors, while depletion of granulin led to a significant upregulation of GzmB and IFNγ expression in CD8$^+$ T cells in response to αPD-1 administration (Figs. 7G,H).

Interestingly, we found in granulin deficient tumors treated with αPD-1 an increased presence of immune stimulatory MAMs that expressed pro-inflammatory markers iNOS, MHC-II, and COX-2 (Fig. 7I; Supplementary Fig. S6B). Reciprocally, these tumors displayed lower numbers of immunosuppressive Ym-1$^+$ and CD206$^+$ MAMs compared to untreated Grn$^{-/-}$ tumors (Fig. 7J; Supplementary Fig. S6C) while total macrophage numbers remained the same (Fig. 7K; Supplementary Fig. S6D). These findings suggest that the observed increase in IFNγ expression by CD8$^+$ T cells in αPD-1 treated granulin deficient mice promotes an immune stimulatory M1-like MAM phenotype, allowing them to further fuel an anti-tumor immune attack.

Although both CSF-1 inhibition and granulin depletion are able to restore cytotoxic T cell infiltration in metastatic tumors, αPD-1 treatment was more effective in granulin deficient tumors (Fig. 7B) compared to WT tumors treated with αCSF-1 (Fig. 4B, d14). Thus, these tumors might still be immunologically different and respond differently to immunotherapy. A recent study revealed that blockade of CSF-1R expressed on cancer associated fibroblasts can induce the accumulation of immunosuppressive Ly6G$^+$ cells, thereby counteracting the therapeutic benefit of CSF-1R and/or αPD-1 inhibition (40). In agreement with these studies, we found that αCSF-1 treatment increases the infiltration of Ly6G$^+$ cells in metastatic tumors, while granulin depletion did not have this effect (Supplementary Fig. S6E). Moreover, while CSF-1 inhibition improved αPD-1 response in WT mice, it rather had a counteracting effect in granulin deficient mice treated with αPD-1 (Supplementary Figs. S6F-J).

Taken together, these findings demonstrate that depletion of granulin dramatically improves the response of metastatic pancreatic tumors to αPD-1 treatment *in vivo* and that targeting a macrophage secreted factor such as granulin might be more effective than targeting macrophages.

To further confirm that the increase in CD8$^+$ T cell infiltration and the improved response to αPD-1 in granulin deficient mice is dependent on reduced fibrosis, we next treated tumor

bearing mice with the Vitamin D analogue Calcipotriol (Cal), an agent which has previously been shown to revert activated stellate cells to quiescence resulting in reduced fibrosis in pre-clinical mouse models (41). Indeed, administration of Cal improved the efficacy of αPD-1 therapy (Supplementary Figs. S7A,B). Tumors treated with Cal had reduced fibrosis (Supplementary Fig. S7C) and decreased hepatic stellate cell activation, while CD8^{+} T cell infiltration was improved (Supplementary Fig. S7D).

Taken together, these data suggest that granulin-induced fibrosis impedes CD8^{+} T cell infiltration and impairs the effectiveness of αPD-1 therapy, and that restoration of CD8^{+} T cell infiltration via granulin depletion/inhibition or possibly via inhibition of other pro-fibrotic factors is a prerequisite for successful αPD-1 therapy in metastatic pancreatic cancer.

Discussion

The data presented herein describe that macrophage-derived granulin is a critical inducer of T cell exclusion in metastatic PDAC, and provide pre-clinical data that support the rational for targeting granulin in combination with immune checkpoint blocker αPD-1 for the treatment of metastatic PDAC (Supplementary Fig. S8A).

During cancer progression, immune evasion is a fundamental mechanism which allows malignant tumor cells to escape destruction by the effector cells of our immune system (1). A recent study described how the presence of tumor infiltrating CD8^{+} T cells together with the presence of neoantigen numbers stratifies PDAC patients with the longest survival; emphasizing the critical role of CD8^{+} T cell in inhibiting PDAC progression (42). In our study we observed that CD8^{+} T cell function and infiltration are lost during metastatic progression. Large human and mouse PDAC tumors, both at the primary (Supplementary Figs. S8B,C) (3) and at the metastatic site (Fig. 1), are poorly infiltrated by CD8^{+} T cells and are characteristically surrounded by high numbers of granulin secreting MAMs and a dense fibrotic stroma (13,20). We could speculate that similar to the metastatic site, macrophage derived granulin promotes CD8^{+} T cell exclusion also at the primary tumor. However, further investigations are needed.

The importance of targeting the immunosuppressive TME in PDAC to obtain clinical benefit from immunotherapy is becoming increasingly more evident (43). However, central to the efficacy of immune checkpoint blockade is the requirement for cytotoxic CD8^{+} T cells to infiltrate into tumors (1,15). Indeed, in our studies we find that metastatic PDAC lesion become sensible to αPD-1 therapy only in the presence of reduced fibrosis mediated by αCSF-1, granulin depletion or calcipotriol treatment.

Dependent on the microenvironmental cytokine milieu, macrophages are not only promoting tumor growth, but they can also critically orchestrate an anti-tumor immune response (30).

Therapies that aim to specifically inhibit the pro-tumorigenic functions of macrophages, while sparing and/or enhancing their tumoricidal activity, could act as an alternative, and perhaps, more efficient approach than therapies that reduce macrophage numbers in tumors (44,45). In this regard, our studies indicate that depletion of granulin is sufficient to restore T

cell infiltration at the metastatic site and that granulin deficient mice show a remarkable response to αPD-1 treatment accompanied by increased numbers of M1- like macrophages. Thus, in the presence of αPD-1, the immune system in granulin deficient mice can access an abundant number of macrophages for their reprogramming towards an immune stimulatory M1-like phenotype, which facilitates the mounting of an effective immune response against cancer.

In conclusion, our studies uncover a mechanism by which metastatic PDAC tumors evade the immune response and provide the rationale for targeting granulin and other factors promoting hepatic fibrosis, in combination with immune checkpoint inhibitors for the treatment of metastatic PDAC.

Supplementary Material

Refer to Web version on PubMed Central for supplementary material.

Acknowledgements

References

1. Chen DS, Mellman I. Oncology meets immunology: the cancer-immunity cycle. Immunity. 2013; 39(1):1–10. [PubMed: 23890059]

2. Fridman WH, Pages F, Sautes-Fridman C, Galon J. The immune contexture in human tumours: impact on clinical outcome. Nature reviews Cancer. 2012; 12(4):298–306. [PubMed: 22419253]

3. Fukunaga A, Miyamoto M, Cho Y, Murakami S, Kawarada Y, Oshikiri T, et al. CD8+ tumor-infiltrating lymphocytes together with CD4+ tumor-infiltrating lymphocytes and dendritic cells improve the prognosis of patients with pancreatic adenocarcinoma. Pancreas. 2004; 28(1):e26–31. [PubMed: 14707745]

4. Galon J, Costes A, Sanchez-Cabo F, Kirilovsky A, Mlecnik B, Lagorce-Pages C, et al. Type, density, and location of immune cells within human colorectal tumors predict clinical outcome. Science. 2006; 313(5795):1960–4. [PubMed: 17008531]

5. Ribas A. Tumor immunotherapy directed at PD-1. The New England journal of medicine. 2012; 366(26):2517–9. [PubMed: 22658126]

6. Topalian SL, Drake CG, Pardoll DM. Immune checkpoint blockade: a common denominator approach to cancer therapy. Cancer cell. 2015; 27(4):450–61. [PubMed: 25858804]

7. Royal RE, Levy C, Turner K, Mathur A, Hughes M, Kammula US, et al. Phase 2 trial of single agent Ipilimumab (anti-CTLA-4) for locally advanced or metastatic pancreatic adenocarcinoma. J Immunother. 2010; 33(8):828–33. [PubMed: 20842054]

8. Brahmer JR, Tykodi SS, Chow LQ, Hwu WJ, Topalian SL, Hwu P, et al. Safety and activity of anti-PD-L1 antibody in patients with advanced cancer. The New England journal of medicine. 2012; 366(26):2455–65. [PubMed: 22658128]

9. Liou GY, Doppler H, Necela B, Edenfield B, Zhang L, Dawson DW, et al. Mutant KRAS-induced expression of ICAM-1 in pancreatic acinar cells causes attraction of macrophages to expedite the formation of precancerous lesions. Cancer discovery. 2015; 5(1):52–63. [PubMed: 25361845]

10. Ireland L, Santos A, Ahmed MS, Rainer C, Nielsen SR, Quaranta V, et al. Chemoresistance in Pancreatic Cancer Is Driven by Stroma-Derived Insulin-Like Growth Factors. Cancer research. 2016; 76(23):6851–63. [PubMed: 27742686]

11. Shree T, Olson OC, Elie BT, Kester JC, Garfall AL, Simpson K, et al. Macrophages and cathepsin proteases blunt chemotherapeutic response in breast cancer. Genes & development. 2011; 25(23): 2465–79. [PubMed: 22156207]

12. Kleeff J, Korc M, Apte M, La Vecchia C, Johnson CD, Biankin AV, et al. Pancreatic cancer. Nat Rev Dis Primers. 2016; 2:16022. [PubMed: 27158978]

13. Jiang H, Hegde S, Knolhoff BL, Zhu Y, Herndon JM, Meyer MA, et al. Targeting focal adhesion kinase renders pancreatic cancers responsive to checkpoint immunotherapy. Nat Med. 2016; 22(8): 851–60. [PubMed: 27376576]

14. Feig C, Jones JO, Kraman M, Wells RJ, Deonarine A, Chan DS, et al. Targeting CXCL12 from FAP-expressing carcinoma-associated fibroblasts synergizes with anti-PD-L1 immunotherapy in pancreatic cancer. Proceedings of the National Academy of Sciences of the United States of America. 2013; 110(50):20212–7. [PubMed: 24277834]

15. Joyce JA, Fearon DT. T cell exclusion, immune privilege, and the tumor microenvironment. Science. 2015; 348(6230):74–80. [PubMed: 25838376]

16. Gajewski TF, Schreiber H, Fu YX. Innate and adaptive immune cells in the tumor microenvironment. Nat Immunol. 2013; 14(10):1014–22. [PubMed: 24048123]

17. Biswas SK, Allavena P, Mantovani A. Tumor-associated macrophages: functional diversity, clinical significance, and open questions. Semin Immunopathol. 2013; 35(5):585–600. [PubMed: 23657835]

18. Noy R, Pollard JW. Tumor-associated macrophages: from mechanisms to therapy. Immunity. 2014; 41(1):49–61. [PubMed: 25035953]

19. Ries CH, Cannarile MA, Hoves S, Benz J, Wartha K, Runza V, et al. Targeting tumor-associated macrophages with anti-CSF-1R antibody reveals a strategy for cancer therapy. Cancer cell. 2014; 25(6):846–59. [PubMed: 24898549]

20. Zhu Y, Knolhoff BL, Meyer MA, Nywening TM, West BL, Luo J, et al. CSF1/CSF1R blockade reprograms tumor-infiltrating macrophages and improves response to T-cell checkpoint immunotherapy in pancreatic cancer models. Cancer research. 2014; 74(18):5057–69. [PubMed: 25082815]

21. Strachan DC, Ruffell B, Oei Y, Bissell MJ, Coussens LM, Pryer N, et al. CSF1R inhibition delays cervical and mammary tumor growth in murine models by attenuating the turnover of tumor-associated macrophages and enhancing infiltration by CD8+ T cells. Oncoimmunology. 2013; 2(12):e26968. [PubMed: 24498562]

22. Mitchem JB, Brennan DJ, Knolhoff BL, Belt BA, Zhu Y, Sanford DE, et al. Targeting tumor-infiltrating macrophages decreases tumor-initiating cells, relieves immunosuppression, and improves chemotherapeutic responses. Cancer research. 2013; 73(3):1128–41. [PubMed: 23221383]

23. DeNardo DG, Brennan DJ, Rexhepaj E, Ruffell B, Shiao SL, Madden SF, et al. Leukocyte complexity predicts breast cancer survival and functionally regulates response to chemotherapy. Cancer discovery. 2011; 1(1):54–67. [PubMed: 22039576]

24. Sperti C, Pasquali C, Piccoli A, Pedrazzoli S. Recurrence after resection for ductal adenocarcinoma of the pancreas. World J Surg. 1997; 21(2):195–200. [PubMed: 8995078]

25. Costa-Silva B, Aiello NM, Ocean AJ, Singh S, Zhang H, Thakur BK, et al. Pancreatic cancer exosomes initiate pre-metastatic niche formation in the liver. Nat Cell Biol. 2015; 17(6):816–26. [PubMed: 25985394]

26. Nielsen SR, Quaranta V, Linford A, Emeagi P, Rainer C, Santos A, et al. Macrophage-secreted granulin supports pancreatic cancer metastasis by inducing liver fibrosis. Nat Cell Biol. 2016; 18(5):549–60. [PubMed: 27088855]

27. Hingorani SR, Wang L, Multani AS, Combs C, Deramaudt TB, Hruban RH, et al. Trp53R172H and KrasG12D cooperate to promote chromosomal instability and widely metastatic pancreatic ductal adenocarcinoma in mice. Cancer cell. 2005; 7(5):469–83. [PubMed: 15894267]

28. Moriya K, Bae E, Honda K, Sakai K, Sakaguchi T, Tsujimoto I, et al. A fibronectin-independent mechanism of collagen fibrillogenesis in adult liver remodeling. Gastroenterology. 2011; 140(5): 1653–63. [PubMed: 21320502]

29. D'Costa Z, Jones K, Azad A, van Stiphout R, Lim SY, Gomes AL, et al. Gemcitabine-Induced TIMP1 Attenuates Therapy Response and Promotes Tumor Growth and Liver Metastasis in Pancreatic Cancer. Cancer research. 2017; 77(21):5952–62. [PubMed: 28765154]

30. Kitamura T, Qian BZ, Pollard JW. Immune cell promotion of metastasis. Nature reviews Immunology. 2015; 15(2):73–86.

31. Mantovani A, Marchesi F, Malesci A, Laghi L, Allavena P. Tumour-associated macrophages as treatment targets in oncology. Nat Rev Clin Oncol. 2017; 14(7):399–416. [PubMed: 28117416]

32. Pyonteck SM, Akkari L, Schuhmacher AJ, Bowman RL, Sevenich L, Quail DF, et al. CSF-1R inhibition alters macrophage polarization and blocks glioma progression. Nat Med. 2013; 19(10): 1264–72. [PubMed: 24056773]

33. Salmon H, Franciszkiewicz K, Damotte D, Dieu-Nosjean MC, Validire P, Trautmann A, et al. Matrix architecture defines the preferential localization and migration of T cells into the stroma of human lung tumors. The Journal of clinical investigation. 2012; 122(3):899–910. [PubMed: 22293174]

34. Elkabets M, Gifford AM, Scheel C, Nilsson B, Reinhardt F, Bray MA, et al. Human tumors instigate granulin-expressing hematopoietic cells that promote malignancy by activating stromal fibroblasts in mice. The Journal of clinical investigation. 2011; 121(2):784–99. [PubMed: 21266779]

35. He Z, Ong CH, Halper J, Bateman A. Progranulin is a mediator of the wound response. Nat Med. 2003; 9(2):225–9. [PubMed: 12524533]

36. Doedens AL, Stockmann C, Rubinstein MP, Liao D, Zhang N, DeNardo DG, et al. Macrophage expression of hypoxia-inducible factor-1 alpha suppresses T-cell function and promotes tumor progression. Cancer research. 2010; 70(19):7465–75. [PubMed: 20841473]

37. Casazza A, Laoui D, Wenes M, Rizzolio S, Bassani N, Mambretti M, et al. Impeding macrophage entry into hypoxic tumor areas by Sema3A/Nrp1 signaling blockade inhibits angiogenesis and restores antitumor immunity. Cancer cell. 2013; 24(6):695–709. [PubMed: 24332039]

38. Fraisl P, Aragones J, Carmeliet P. Inhibition of oxygen sensors as a therapeutic strategy for ischaemic and inflammatory disease. Nat Rev Drug Discov. 2009; 8(2):139–52. [PubMed: 19165233]

39. Zhang H, Qian DZ, Tan YS, Lee K, Gao P, Ren YR, et al. Digoxin and other cardiac glycosides inhibit HIF-1alpha synthesis and block tumor growth. Proceedings of the National Academy of Sciences of the United States of America. 2008; 105(50):19579–86. [PubMed: 19020076]

40. Kumar V, Donthireddy L, Marvel D, Condamine T, Wang F, Lavilla-Alonso S, et al. Cancer-Associated Fibroblasts Neutralize the Anti-tumor Effect of CSF1 Receptor Blockade by Inducing PMN-MDSC Infiltration of Tumors. Cancer cell. 2017; 32(5):654–68 e5. [PubMed: 29136508]

41. Sherman MH, Yu RT, Engle DD, Ding N, Atkins AR, Tiriac H, et al. Vitamin d receptor-mediated stromal reprogramming suppresses pancreatitis and enhances pancreatic cancer therapy. Cell. 2014; 159(1):80–93. [PubMed: 25259922]

42. Balachandran VP, Luksza M, Zhao JN, Makarov V, Moral JA, Remark R, et al. Identification of unique neoantigen qualities in long-term survivors of pancreatic cancer. Nature. 2017; 551(7681): 512–16. [PubMed: 29132146]

43. Anderson KG, Stromnes IM, Greenberg PD. Obstacles Posed by the Tumor Microenvironment to T cell Activity: A Case for Synergistic Therapies. Cancer cell. 2017; 31(3):311–25. [PubMed: 28292435]

44. Bronte V, Murray PJ. Understanding local macrophage phenotypes in disease: modulating macrophage function to treat cancer. Nat Med. 2015; 21(2):117–9. [PubMed: 25654601]

45. Quail DF, Joyce JA. Microenvironmental regulation of tumor progression and metastasis. Nat Med. 2013; 19(11):1423–37. [PubMed: 24202395]
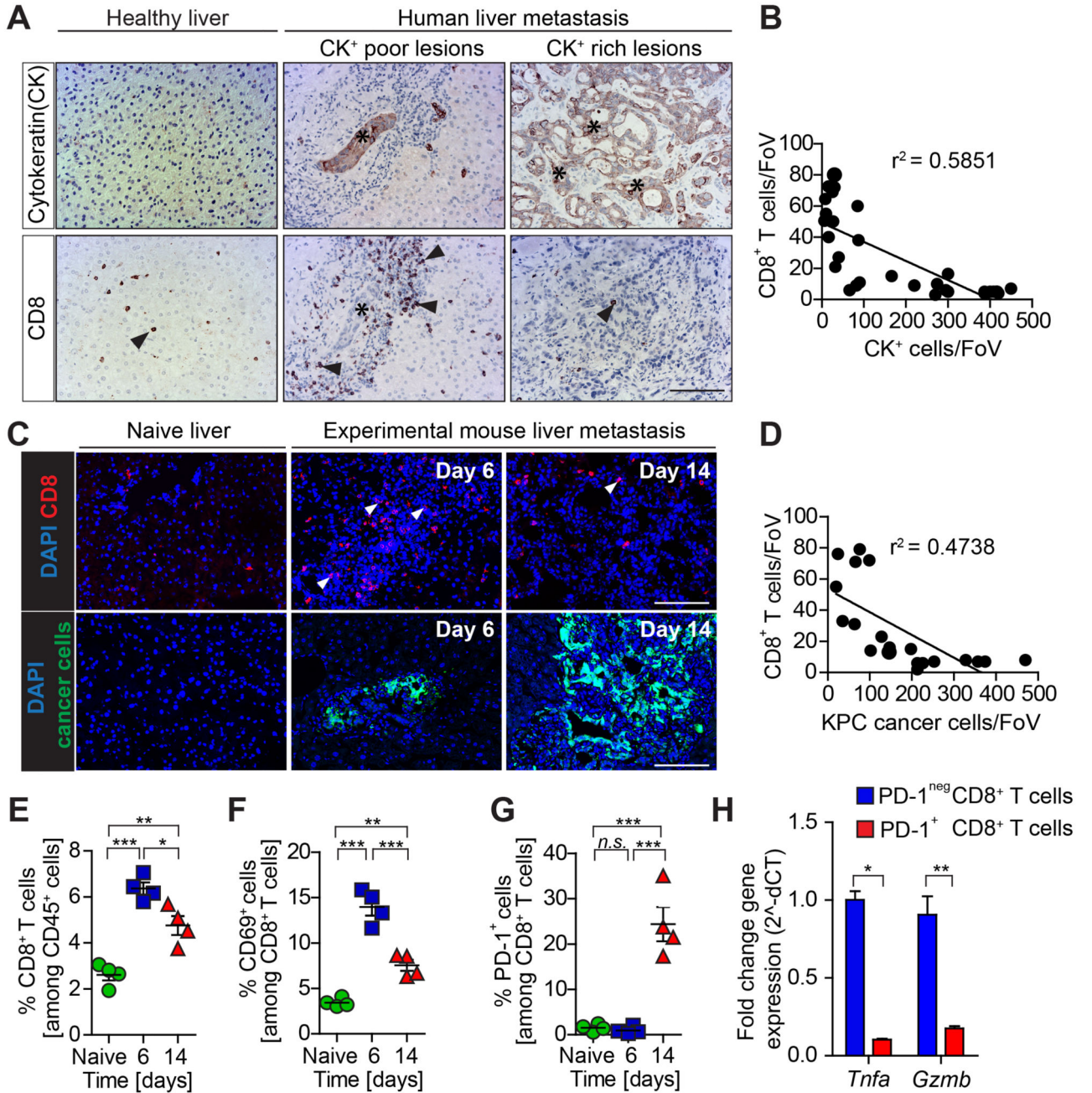
Figure 1. CD8+ T cell infiltration and activation is lost during metastatic PDAC progression
(**A-B**) Immunohistochemistry images and quantification of cytokeratin (CK)+ metastatic cancer cells and cytotoxic T cells (CD8+) infiltration in human serial tissue sections (n = 10 metastatic PDAC; n = 5 healthy; each metastatic PDAC tissue section contained multiple lesions. Individual lesions were captured by one field of view (FoV). Dots represent the relationship between CD8+ T cell numbers and CK+ cell numbers in each lesion; (**C-H**) Liver metastasis was induced by intrasplenic implantation of KPC$^{zsGreen/luc}$ cancer cells. Livers were resected from metastatic mice after 6 and 14 days. (C-D) Individual lesions

were captured by one FoV. Dots represent the relationship between CD8$^+$ T cell numbers and KPC$^{zsGreen/luc}$ cancer cell numbers in each lesion (n=4 mice / time point, five FoV quantified / mouse) (E) Percentage of CD8$^+$ T cells, (F) CD69$^+$ CD8$^+$ T cells, (G) and PD-1$^+$ CD8$^+$ T cells over time assessed by flow cytometry analysis. (H) Quantification of *Tnfa and Gzmb* mRNA levels in PD-1$^+$ and PD-1^{neg} CD8$^+$ T cells isolated by fluorescence activated cell sorting (FACS) from livers resected at day 14. Scale bars = 100μm; ***, *P*<0.001; **, *P* < 0.01; *, *P* < 0.05; n.s., not significant, by unpaired t-test and/or Bonferroni multiple comparison.
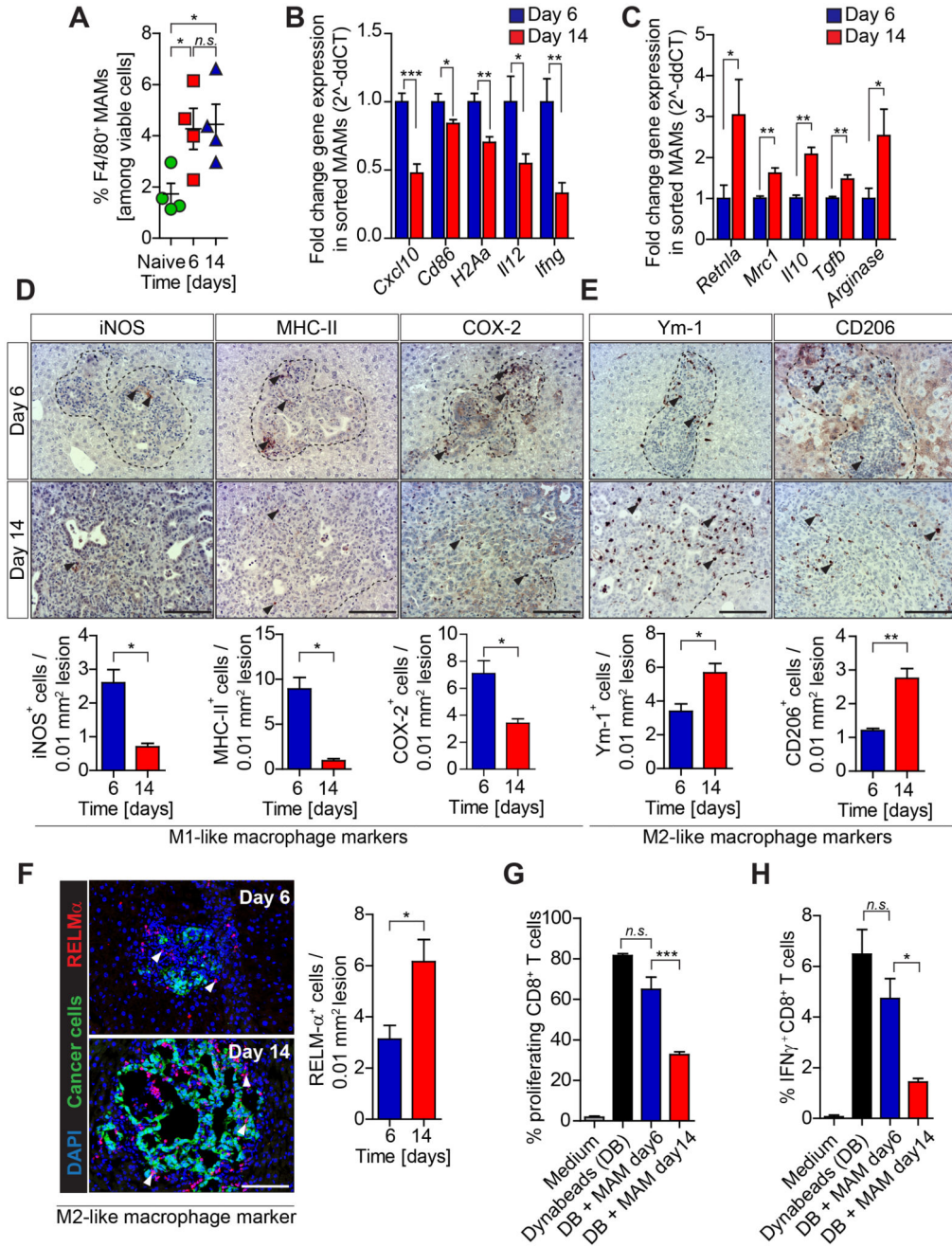
Figure 2. Immune suppressive macrophages accumulate in established PDAC metastasis.
Liver metastasis was induced by intrasplenic implantation of KPC [luc/zsGreen] cancer cells.
Livers were resected 6 and 14 days (n= 4 mice / time point) and analyzed. (**A**) Flow
cytometry quantification of F480^{+} cells in naïve and metastatic resected livers. (**B-C**) M1
and M2-macrophage associated genes expression in FACS isolated MAMs by qPCR. (**D**)
Immunohistochemistry images and quantification of M1-like MAM markers and (**E**) M2-
like MAM markers. (**F**) Immunofluorescent images and quantification of RELMα[+] M2-like
macrophages clustering around metastatic PDAC cells (zsGreen[+]).(**G-H**) MAMs isolated

from resected livers were tested for their ability to (G) suppress CD28/CD3 Dynabeads (DB) stimulated splenic CD8$^+$ T cell proliferation (CFSE dilution) (H) and activation (IFNγ level) (data are mean ± SD of 4 independent experiments). Scale bars= 100μm; ***, $P<0.001$; **, $P< 0.01$; *, $P< 0.05$; n.s., not significant, by unpaired t-test and/or Bonferroni multiple comparison.
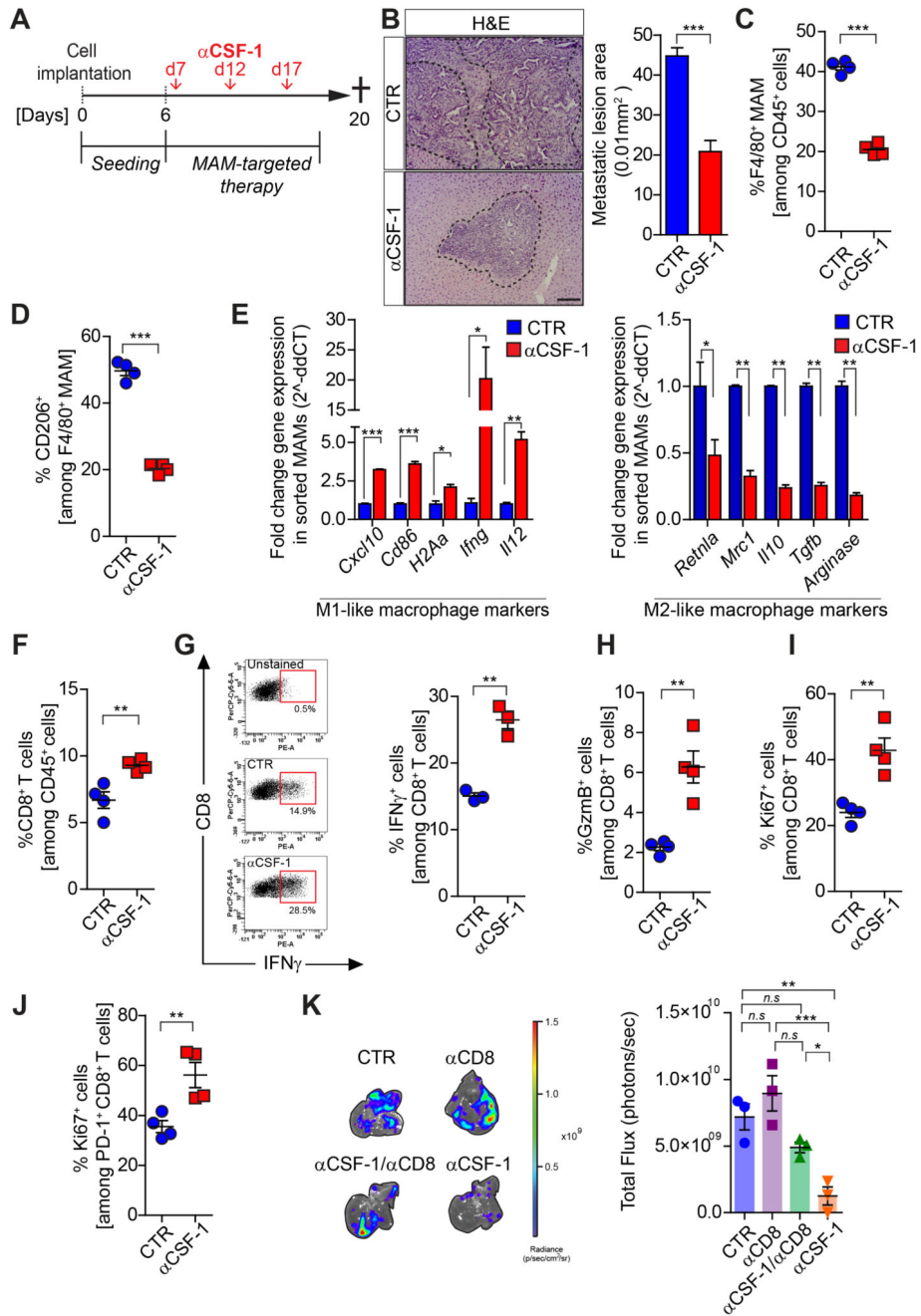
Figure 3. Pharmacological blockade of CSF-1 reprograms MAMs and reinvigorates CD8^{+} T cell functions

Liver metastasis was induced by intrasplenic implantation of KPC[zsGreen/luc] cells. After 7 days mice were treated with IgG control (Ctr) or αCSF-1 antibody. Metastatic livers were resected at day 20 and analyzed by haematoxylin and eosin (H&E) staining (n=6 mice/group) and by flow cytometry (n=4 mice/group). (**A**) Schematic illustration of the experiment. (**B**) H&E images and quantification. (**C**) Total and (**D**) M2-like (CD206^{+}) MAMs. (**E**) M1-like and M2-like macrophage genes expression analysis in MAMs (**F**)

Quantification of CD8$^+$ T cells. (**G**) Representative dot plot and quantification of IFNγ levels in CD8$^+$ T cells (n = 3 mice /group); Quantification of (**H**) Granzyme B$^+$ (GzmB) cells, (**I**) proliferating (Ki67$^+$) cells among total CD8$^+$ T cells and among (**J**) PD-1$^+$ CD8$^+$ T cells. (**K**) Metastatic tumor burden in mice treated with αCD8 and αCSF-1 alone or in combination (n = 3 mice /group).

Scale bars = 100μm; ***, *P*<0.001; **, *P* < 0.01; *, *P* < 0.05; n.s., not significant, by unpaired t-test and/or Bonferroni multiple comparison.
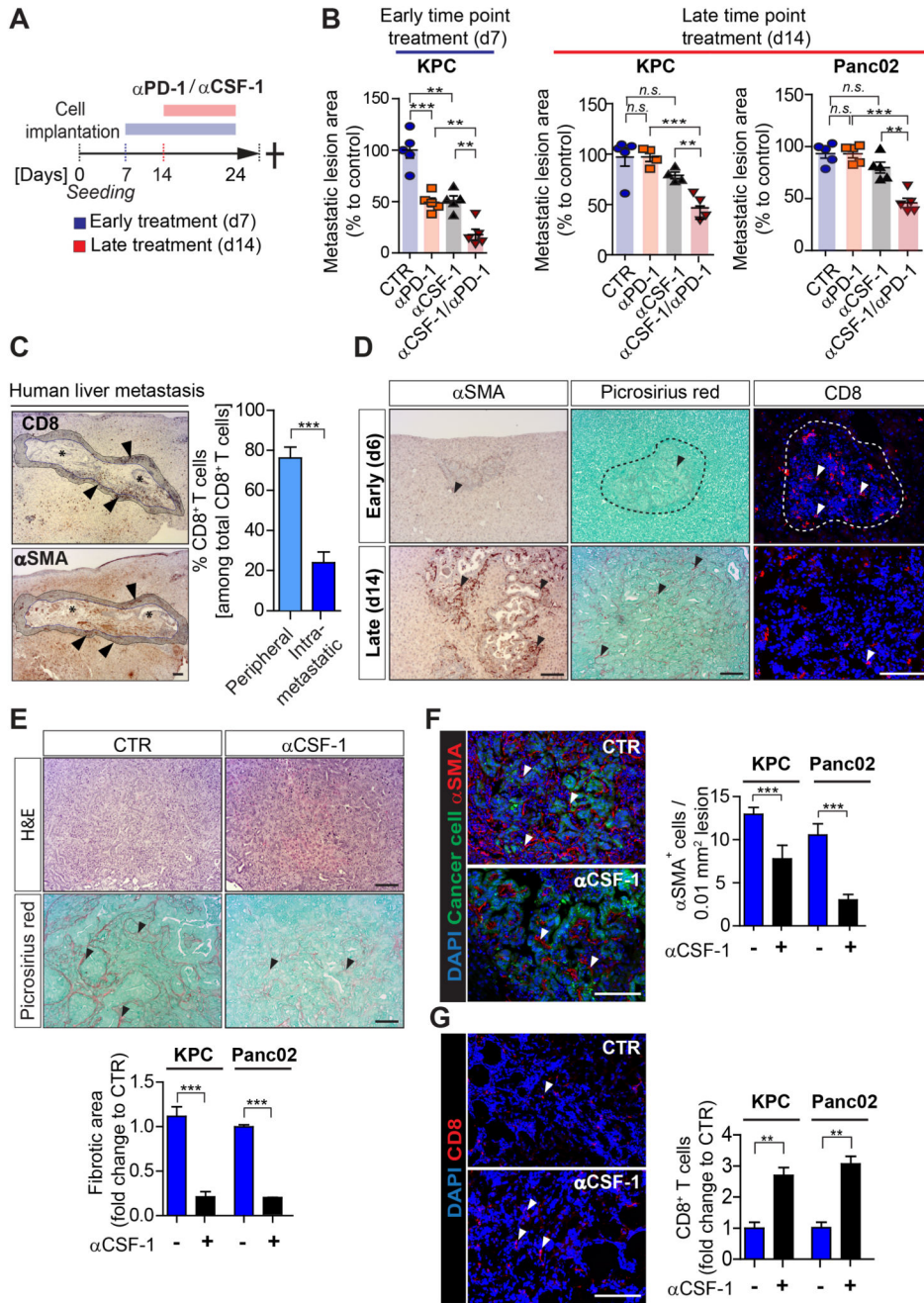
Figure 4. CSF-1 inhibition reduces desmoplasia and sensitizes metastatic PDAC to αPD-1 treatment

Liver metastasis was induced by intrasplenic implantation of KPC[zsGreen/luc] cells or Panc02[zsGreen/luc] cancer cells. Cohorts were treated with control IgG, αCSF-1 and αPD-1, alone or in combination. Treatment started at day 7 (d7) or at day 14 (d14) (n = 4 or 5 mice / group). (**A**) Schematic representation of the treatment regimen. (**B**) Percentage of average change in metastatic lesion area compared to control in response to treatment assessed by H&E staining at endpoint. (**C**) Immunohistochemistry images of CD8^{+} T cells and
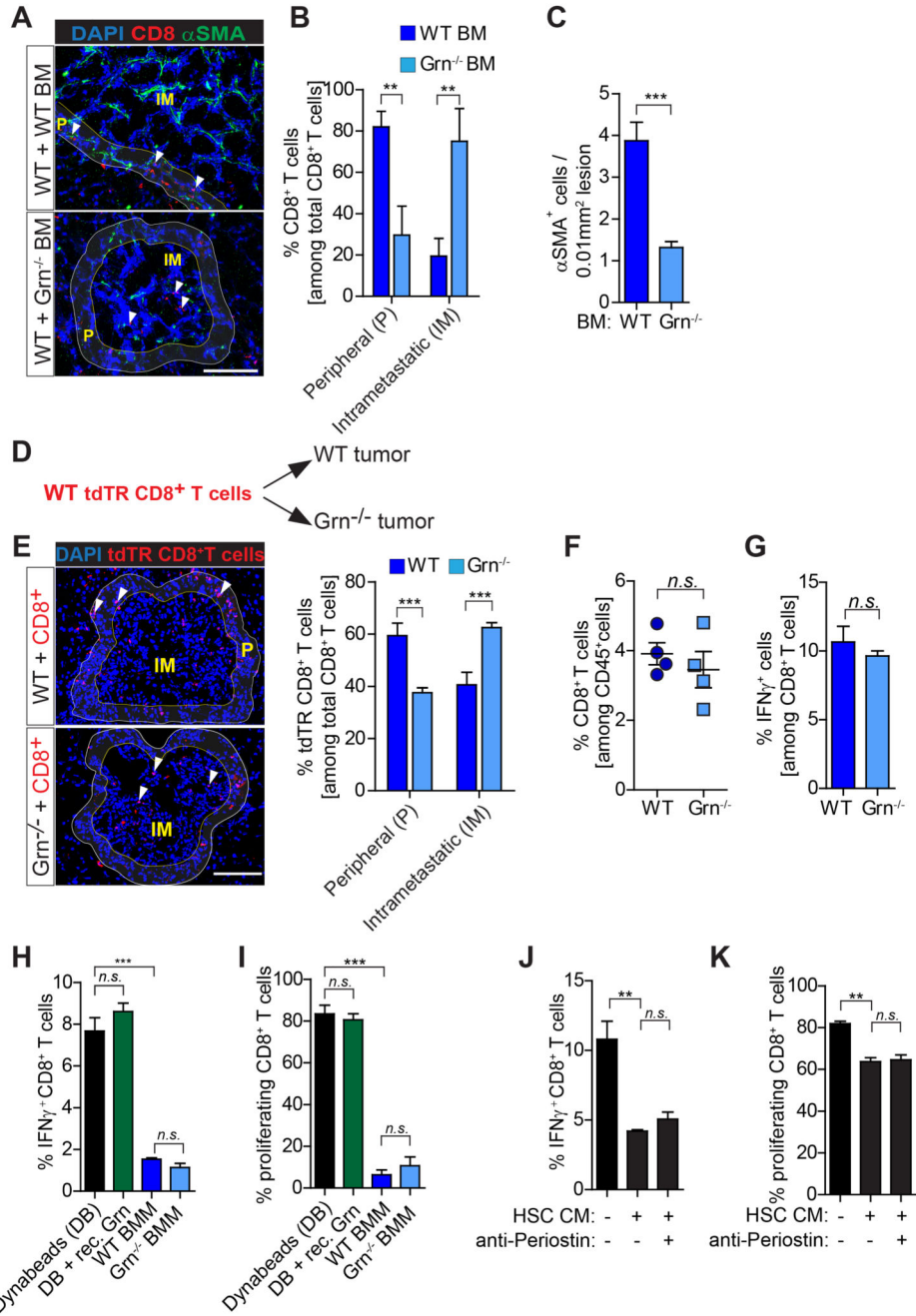
myofibroblasts (αSMA$^+$) in human PDAC metastatic livers and quantification of perimetastatic (P) and intrametastatic (IM) CD8$^+$ T cells (n= 6 patients). (**D**) Liver metastasis was induced by intrasplenic implantation of KPC$^{zsGreen/luc}$ cancer cells. Livers were resected after 6 and 14 days and assessed by αSMA$^+$ (myofibroblasts), Picrosirius red (collagen deposition) and CD8$^+$ T cell staining. (**E-G**) Images and relative quantification of (E) picrosirius red and H&E staining of sequential tumor sections showing area occupied by fibrotic stroma, (F) myofibroblasts (αSMA$^+$, red) cell frequency and (G) infiltrating CD8$^+$ T cells in liver tissue sections of mice treated at d14 with IgG control or αCSF-1. Quantification of staining is referred to metastatic tumor generated by KPC $^{zsGreen/luc}$ or Panc02 $^{zsGreen/luc}$ cancer cells implantation. Images are representative of KPC $^{zsGreen/luc}$ cancer cells derived liver metastatic lesions (n= 4 or 5 mice / group; additional treatment groups are shown in Supplementary Fig. S4). Scale bars= 100μm; ***, P<0.001; **, P< 0.01; *, P< 0.05; n.s., not significant, by unpaired t-test and/or Bonferroni multiple comparison.
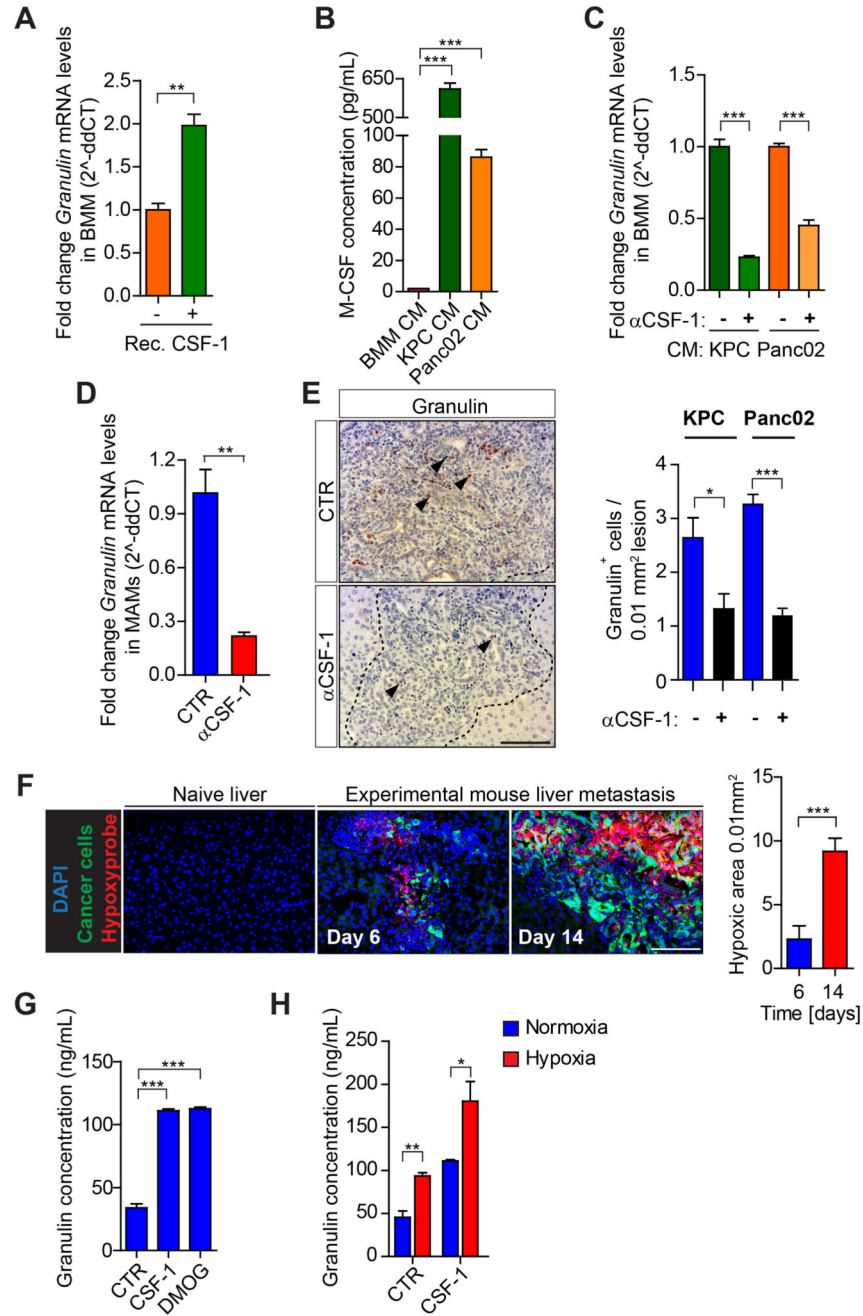
Figure 5. Hypoxia amplifies CSF-1-induced granulin expression in macrophages
(**A**) Quantification of *Granulin* expression by qPCR in primary bone marrow derived
macrophages (BMMs) unstimulated and exposed to recombinant CSF-1. (**B**) ELISA
quantification of CSF-1 protein levels in conditioned medium (CM) generated from BMMs,
and KPC and Panc02 pancreatic cancer cells. (**C**) Quantification of *Granulin* expression by
qPCR in BMMs exposed to KPC and Panc02 conditioned media (CM) in the presence of
IgG control (Ctr) or neutralizing αCSF-1 mAb. (**D**) Quantification of *Granulin* expression in
MAMs from KPC^zsGreen/luc induced metastatic tumors treated with IgG control (Ctr) or

αCSF-1. (**E**) Immunohistochemistry images and quantification of granulin in KPC[zsGreen/luc] or Panc02 [zsGreen/luc] tumor bearing mice treated with IgG control (Ctr) or αCSF-1 (n = 4 mice). (**F**) Representative images and quantification of hypoxic areas surrounding metastatic KPC[zsGreen/luc] cells (zsGreen[+]) assessed by Hypoxyprobe™-1 (n= 3 mice / group). (**G-H**) ELISA quantification of (G) granulin protein level in unstimulated BMMs (Ctr), and BMMs exposed to recombinant murine CSF-1 or DMOG for 24 hours and (H) granulin protein level in BMMs cultured for 24 hours under normoxic and hypoxic conditions in presence or absence of recombinant murine CSF-1. In A-C, G-H data are mean ± SD of 3 independent experiments. Scale bars= 100μm; ***, P<0.001; **, P< 0.01; *, P< 0.05; n.s., not significant, by unpaired t-test.

Figure 6. CD8+T cells intra-metastatic infiltration but not activity is increased in granulin depleted mice

(**A-C**) Liver metastasis was induced by intrasplenically implantation of KPC cells into chimeric WT+ WT BM and WT+ Grn$^{-/-}$ BM mice. Entire livers were resected 14 days later and analyzed. (A) Immunofluorescence images of CD8+ T cells and αSMA+ myofibroblasts. Intrametastatic (IM) and peripheral areas (P) are indicated. (B) Quantification of peripheral (P) and intrametastatic (IM) CD8+ T cells. (C) Quantification of αSMA+ cells (WT BM, n= 5; Grn$^{-/-}$ BM, n= 6). (**D-E**) Adoptive transfer of tdTR CD8+ T

cells into metastasis bearing WT and Grn^{-/-} mice (D) Schematic illustration of the experiment. (E) Immunofluorescence images and quantification of tdTR CD8^{+} T cells (red) in perimetastatic (P) and intrametastatic (IM) regions (n= 3 mice / group). (**F-G**) KPC cells were intrasplenically implanted in mice to induce liver metastasis in WT and Grn^{-/-} mice. Livers were resected after 14 days and analyzed (n= 4 WT and n= 4 Grn^{-/-} mice). (F) Flow cytometry quantification of CD8^{+} T cell number and (G) IFNγ^{+} CD8^{+} T cell. (**H-I**) Bone marrow isolated macrophages (BMMs) derived from WT and Grn^{-/-} mice and recombinant granulin (rec. Grn) were tested for the capacity of suppress splenic CD8^{+} T cell (H) activation (IFNγ expression levels) and (I) proliferation (CFSE dilution). (**J-K**) Conditioned medium (CM) generated from activated hepatic stellate cells (HSC) was used to validate the (J) activation (IFNγ expression levels) and (K) proliferation (CFSE dilution) of splenic CD8^{+} T cell in the presence or absence of a periostin neutralizing antibody. In H-K data are mean ± SD of 3 independent experiments. Scale bars= 100μm; ***, P<0.001; **, P< 0.01; *, P< 0.05; n.s., not significant, by unpaired t-test and/or Bonferroni multiple comparison.
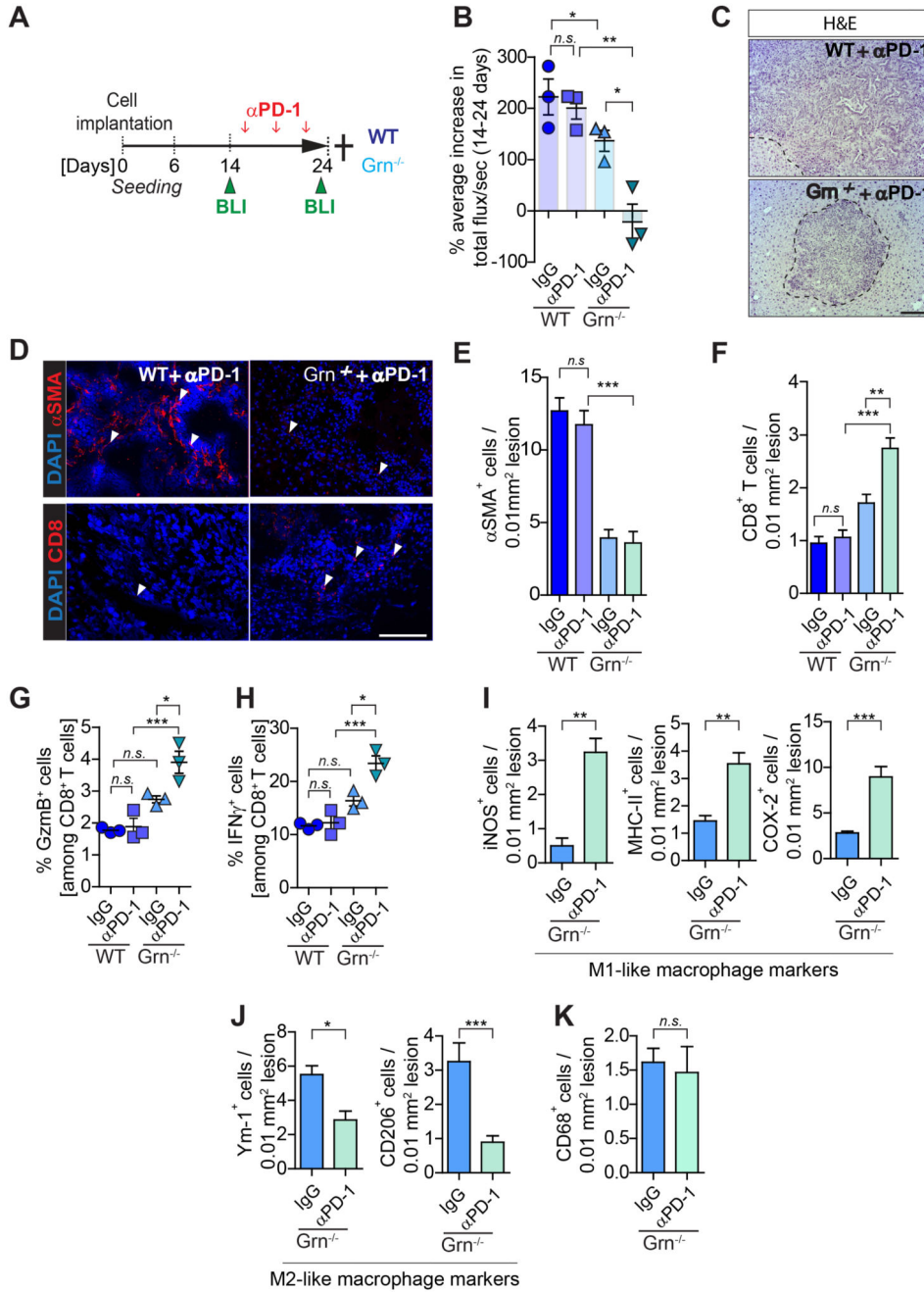
Figure 7. Depletion of granulin restores response of metastatic PDAC to αPD-1 therapy
Liver metastasis was induced by intrasplenic implantation of KPC$^{zsGreen/luc}$ cells in WT and Grn$^{-/-}$ mice. Mice were treated with control IgG or αPD-1. Change in tumor burden was quantified by *in vivo* BLI. (n= 3 mice/group). (**A**) Schematic illustration of the experiment. (**B**) Change in metastatic tumor burden (total flux/sec). (**C**) H&E images of αPD-1 treated cohorts. Metastatic lesions are delineated with dashed lines. (**D**) Immunofluorescence images of myofibroblasts (αSMA$^+$) and CD8$^+$ T cell staining of sequential liver sections from WT and Grn$^{-/-}$ mice treated with αPD-1. (**E-F**) Quantification of myofibroblasts

(αSMA$^+$) accumulation and CD8$^+$ T cell infiltration as described in D. Quantifications of (**G**) Granzyme B (GzmB$^+$) and (**H**) IFNγ$^+$ CD8$^+$ T cells by flow cytometry analysis. (**I-K**) Immunohistochemistry images and quantification of cells positive for (I) pro-inflammatory M1-like (iNOS, MHC-II, COX-2) MAMs, (J) anti-inflammatory M2-like (Ym-1, CD206) MAMs and (K) total (CD68) MAMs markers. Scale bars= 100μm; ***, P<0.001; **, P< 0.01; *, P< 0.05; n.s., not significant, by unpaired t-test and/or Bonferroni multiple comparison.